UDC 621.45.035.01:621.794.4 **doi: 10.32620/reks.2026.2.04**

Oleksandr SHORINOV, Nina SAVCHENKO, Oleg TRYFONOV, Olga SHYPUL

National Aerospace University "Kharkiv Aviation Institute", Kharkiv, Ukraine

COMPUTATIONAL ANALYSIS OF COLD SPRAY NOZZLE DESIGN'S EFFECT ON PARTICLE ACCELERATION

The subject of this *article is the computational analysis of the effect of nozzle geometry on gas dynamics and particle acceleration in cold gas dynamic spraying (CGDS).* ***This study aims*** *to compare the performance of conventional conical nozzles and Method of Characteristics (MOC)-based bell-shaped nozzles in accelerating particles to the critical velocities required for effective coating deposition.* ***The tasks*** *to be solved are as follows: design and model conical and MOC nozzles; conduct CFD simulations of compressible two-phase gas–particle flows in both geometries; analyze velocity, pressure, and temperature distributions along the nozzle and jet regions; and evaluate particle acceleration and velocity distribution for aluminum powder.* ***The following methods were used****: numerical modeling of gas–particle flow employing the Navier–Stokes equations with the RNG k–ε turbulence model in ANSYS Fluent 2025 R1, along with Lagrangian particle tracking; computational design of nozzles using MATLAB code based on the Method of Characteristics; and comparison of flow fields and particle dynamics between nozzle configurations.* ***The results*** *show that both nozzles operate under underexpanded jet conditions, but the MOC nozzle accelerates the carrier gas and particles earlier, resulting in more uniform velocity fields and reduced velocity lag between the gas and the dispersed phase. For 25 μm aluminum particles, the MOC nozzle achieves higher particle velocities than the conical nozzle, indicating greater potential for plastic deformation and improved coating adhesion. Additionally, higher exit gas velocities and more stable jet structures were observed in the MOC nozzle, despite the presence of more pronounced boundary-layer vorticity.* ***Conclusions.*** *The scientific novelty of the results lies in establishing the gas-flow acceleration patterns with aluminum powder particles in conical and MOC-based nozzles, optimized for aluminum deposition at 2.5 MPa gas pressure and 650 °C. The MOC-based nozzle enables earlier gas expansion and a more stable free-jet structure, thereby achieving a higher, significantly more uniform powder particle velocity than the conical nozzle under identical spraying conditions.*

Keywords*:* CFD simulation, mathematical modeling, gas flow, supersonic nozzle, ANSYS Fluent, spraying, coating.

1. Introduction

1.1. Motivation

Cold Gas Dynamic Spraying (CGDS) is currently one of the most promising technologies for the application of functional coatings. This process is based on the kinetic acceleration of powder particles using compressed gas, which enables the deposition of strong and wear-resistant layers without a significant thermal impact on the substrate material [1, 2]. The absence of heating opens wide opportunities for the processing of thermally sensitive surfaces, which is particularly relevant for modern industrial sectors.

One of the key components of CGDS systems is the nozzle, which shapes the gas flow and directly affects the particles' kinetic characteristics. As noted in previous studies [3, 4], nozzle geometry determines not only the gas velocity but also the pressure and turbulence level, and consequently, the efficiency of kinetic energy transfer to powder particles. In turn, this directly influences the quality of the formed coating.

In the scientific literature, two main types of nozzle geometry are distinguished: straight (in particular, conical) and curved (bell-shaped). According to authors of studies [5, 6], straight nozzles are characterized by simple construction, whereas curved nozzles allow for more stable and directed acceleration of the gas flow through adiabatic expansion. In the context of CGDS, this leads to improved kinetic properties of particles and better coating quality.

Although many researchers have focused on individual aspects of nozzles with different geometries, a comprehensive comparison of their effectiveness considering hydrodynamic and operational characteristics remains insufficiently studied [7]. Therefore, this study aims to perform a systematic analysis of the influence of straight and curved nozzles on gas flow parameters, particle velocity distribution, and coating quality.

1.2. State of the art

Studying adiabatic gas expansion in CGDS nozzles is fundamental for understanding the formation of high-speed flows. Dykhuizen and Smith [1] emphasized that

ISSN 1814-4225 (print)
ISSN 2663-2012 (online)

minimizing hydraulic losses and turbulence is critical for improving the efficiency of kinetic energy transfer from gas to particles.

Bernard et al. [2] demonstrated that conical nozzles create a more uniform velocity profile across the jet cross-section. This ensures more even particle acceleration and improves coating adhesion, whereas straight nozzles tend to form peak velocities with significant fluctuations, negatively affecting spray quality.

Computational fluid dynamics (CFD) modeling performed by Grujicic et al. [3] showed that the optimal expansion angle of conical nozzles is within 7–10°, which provides maximum gas velocity with minimal pressure losses. This parameter is crucial for flow stability and particle acceleration.

In a review of modern nozzle designs, the authors of [4] investigated a convergent-divergent barrel nozzle using Ansys Fluent software. The divergent-barrel shape of the nozzle results in higher particle velocity than the standard one.

Shorinov et al. [5] focused on the influence of powder properties on their acceleration and heating in a low-pressure cold spray nozzle (up to 1.0 MPa). The different powder feeding points are preferable for a multicomponent powder composition to achieve the required acceleration.

Gabor et al. [6] reported a detailed comparison of gas dynamics and powder particle motion in cold gas dynamic spraying with round and rectangular nozzle outlets. The round shape of the nozzle shows a more uniform particle velocity within the nozzle channel.

The significant impact of nozzle expansion angle on turbulence is highlighted in [7], where angles less than 5° are associated with laminar flow and higher concentrations of fast particles, whereas angles above 12° lead to turbulent vortices, reducing spraying efficiency. Concurrently, the authors showed that conical nozzles form a more concentrated flow with less velocity variability, enhancing process productivity, especially with smooth geometric transitions, minimizing pressure losses.

Grujicic et al. [8] discussed the important relationship between powder particle size and optimal cone angle. For fine particles, an angle of around 8° is recommended, whereas for larger particles, an angle of up to 12° is recommended to maximize kinetic energy and reduce nozzle wear.

Karimi et al. [9] numerically demonstrated that a conical geometry reduces turbulence at the nozzle outlet, improving process stability, while [10] showed reduced noise and vibration, positively affecting industrial operating conditions.

Coatings deposited through curved nozzles are noted for more uniform thickness and improved adhesion, as confirmed by Krampe and Kuhlenkötter [11]. The visualization of particle velocity in [12] confirms the flow stability and directionality in conical nozzles.

Energy consumption reduction by 15%–20% using optimized conical nozzles was experimentally proven by Kun et al. [13]. The genetic algorithm optimization of the nozzle shape described in [14] indicates that a smooth transition with an angle of approximately 9° minimizes hydraulic losses and maximizes the flow velocity.

The simplicity of manufacturing straight nozzles remains an advantage; however, as Sakaki et al. [15] emphasized, they have limited flexibility in parameter adjustment, reducing their effectiveness in complex production tasks.

Numerous studies have confirmed the stability of pressure and gas flow velocity in curved nozzles [16, 17], which is a key factor for achieving an optimal balance between particle kinetic energy and coating uniformity [18].

Multiphysics models described by Murphy et al. [19] reveal the impact of nozzle geometry not only on hydrodynamics but also on thermal flow characteristics, which are important for controlling coating properties.

Alonso et al. [20] confirmed noise and vibration reduction due to optimized conical nozzles, improving working conditions and extending system service life.

Finally, Yin et al. [21] demonstrated that optimal nozzle expansion angles of 7–10° yield maximum gas flow velocity with minimal energy loss, which is critical for CGDS efficiency.

Thus, the analysis of the scientific literature confirms that nozzle geometry is one of the key factors determining the dynamic spraying efficiency of cold gas. Despite numerous studies, a comprehensive comparison of straight and curved nozzles, accounting for their effects on flow hydrodynamics, particle kinetic parameters, and coating quality, remains to be investigated. This justifies the relevance and necessity of a systematic study.

1.3. Objectives and tasks

The compressible, turbulent, and complex behavior of gas-particle flow within supersonic nozzles makes experimental studies of particle acceleration and gas-particle interactions particularly difficult. Therefore, numerical analysis and computational modeling have become indispensable tools for investigating these phenomena.

This study aims to compare the performance of a conventional conical nozzle and a Method of Characteristics (MOC)-based nozzle in terms of gas dynamics and particle acceleration efficiency in dynamic spraying of cold gas. The specific objective is to determine which nozzle geometry, under identical initial gas parameters, ensures superior key gas-dynamic characteristics of the CGDS process: achieving maximum exit velocities for the carrier gas and powder particles, uniformity of the velocity distribution, and flow stability during discharge into the free-jet region, which will ultimately enhance the intensity of plastic deformation and the adhesion strength of the coating to the substrate.

To achieve this goal, it is necessary to solve the following tasks within the framework of this publication:

1. to design and generate the geometry of conical and MOC nozzles using analytical methods and the Method of Characteristics;
2. to perform CFD simulations of compressible two-phase gas–particle flow in both nozzle configurations using ANSYS Fluent;
3. to analyze gas flow parameters (velocity, pressure, temperature) and particle dynamics within the nozzle and in the free jet region;
4. to compare particle acceleration efficiency and velocity distributions obtained in both nozzle designs.

The article is organized as follows: Section 2 presents the research methodology, including the governing equations of compressible gas flow, turbulence model, particle dynamics modeling, and nozzle design procedure. Section 3 discusses the results of CFD simulations for both nozzle types, focusing on the gas flow structure and particle trajectories, and then presents a comparative analysis of the particle velocity distributions at the nozzle exit. Section 4 concludes with a summary of the main findings, highlighting the advantages of MOC-based nozzles over conical ones, and outlining future research directions for further optimization and experimental validation.

2. Methods of research

2.1. Numerical methodology

Basic equations

The Navier–Stokes equations govern the behavior of a compressible gas flow. The governing equations describing the conservation of mass, momentum, energy, and turbulent kinetic energy are presented below. The continuity equation can be expressed as follows:

$$\frac{\partial \rho}{\partial t} + \frac{\partial}{\partial x_i}(\rho u_i) = 0, \quad (1)$$

where ρ denotes the gas density, u_i represents the velocity component in the $i-$th direction, and t is the time.

The momentum conservation equation is formulated as follows:

$$\frac{\partial}{\partial t}(\rho u_i) + \frac{\partial}{\partial x_j}(\rho u_i u_j) = \frac{\partial}{\partial x_j}\left[-P + \mu_{eff}\left(\frac{\partial u_i}{\partial x_j} + \frac{\partial u_j}{\partial x_i}\right)\right] + S_M, \quad (2)$$

where P is the pressure, including the contribution of turbulent normal stresses, and S_M is the source term describing the exchange of mass and momentum between the dispersed and gas phases.

The effective turbulent viscosity, μ_{eff} , is defined as:

$$\mu_{eff} = \rho C_\mu \frac{k^2}{\epsilon}, \quad (3)$$

where $C\mu$ = 0,0845 [22].

The transport equations for the turbulent kinetic energy k and its dissipation rate ϵ are solved in the following form:

$$\frac{\partial}{\partial t}(\rho k) + \frac{\partial}{\partial x_i}(\rho k u_i) = \frac{\partial}{\partial x_j}\left[\mu_{eff}\alpha_k\left(\frac{\partial k}{\partial x_j}\right)\right] + G_k + G_b - Y_M + S_k - \rho \epsilon, \quad (4)$$

$$\frac{\partial}{\partial t}(\rho \epsilon) + \frac{\partial}{\partial x_i}(\rho \epsilon u_i) = \frac{\partial}{\partial x_j}\left[\mu_{eff}\alpha_\epsilon\left(\frac{\partial \epsilon}{\partial x_j}\right)\right] + C_{1\epsilon}\frac{\epsilon}{k}(G_k + C_{3\epsilon}G_b) - C_{2\epsilon}\rho\frac{\epsilon^2}{k} + S_\epsilon - R_\epsilon, \quad (5)$$

where $C_{1\epsilon}, C_{2\epsilon}$ and $C_{3\epsilon}$ are empirical coefficients of the turbulence model [22]. The parameters α_ϵ and α_k represent the inverse effective Prandtl numbers associated with ϵ and k respectively. The terms G_k and G_b account for turbulence generation caused by velocity gradients and buoyancy effects, whereas S_k and S_ϵ correspond to user-specified source terms.

The additional contribution R_ϵ is defined as:

$$R_\epsilon = \frac{C_\mu \rho \eta^3\left(1-\frac{\eta}{\eta_0}\right)}{1+\beta\eta^3}\frac{\epsilon^2}{k}, \quad (6)$$

where $\eta \equiv Sk/\epsilon$, S denotes the magnitude of the mean strain-rate tensor, while $\eta_0 = 4{,}33$ and $\beta = 0{,}012$ are model constants [22].

The Reynolds-averaged energy equation is formulated in terms of the total energy (total enthalpy), h_{tot}, which is expressed as follows:

$$\frac{\partial}{\partial t}(\rho h_{tot}) - \frac{\partial P}{\partial t} + \frac{\partial}{\partial x_j}(\rho u_j h_{tot}) = \frac{\partial}{\partial x_j}\left(\lambda\frac{\partial T}{\partial x_j} + \frac{\mu_t}{Pr_t}\frac{\partial h}{\partial x_j}\right) + + \frac{\partial}{\partial x_j}\left[u_i(\tau_{ij} - \rho\overline{u_i u_j})\right] + S_T, \quad (7)$$

where Pr_t is the turbulent Prandtl number, S_T denotes the source term associated with heat transfer between the gas flow and the dispersed particles, τ denotes the stress tensor, and λ is the thermal conductivity.

The enthalpy is associated with the total energy of the system, accounting for the viscous work.

$$h_{tot} = C_v T + \frac{1}{2}(u_i u_j) + k. \quad (8)$$

For dilute particle-laden flows, the source terms S_m and S_T in equations (2) and (7) are neglected because of the relatively low particle concentration. This simplification is applicable to flow regimes characterized by high Stokes numbers and a small momentum coupling parameter, Π_{mom} [23]. The momentum coupling parameter is defined by the following expression:

ISSN 1814-4225 (print)
ISSN 2663-2012 (online)

$$\Pi_{mom} = \frac{z}{\frac{\rho_p d^2 V}{18\mu_g L}+1}, \qquad (9)$$

where the subscripts p and g identify the particle and gas phases, respectively. The parameter d denotes the particle diameter; L is the characteristic length of the system (for example, the nozzle diameter); and Z represents the powder-to-gas mass flow ratio.

Considering that $\rho_g \ll \rho_p$ and the powder feed rate in this study was 0.6 g/s, the solid phase volume fraction is below 1%, confirming its negligible effect on the overall flow. Particle–particle interactions were neglected owing to the extremely low particle concentration within the flow.

A Lagrangian approach was used to model the solid phase, treating particles as separate entities [23]. A pressure-based solution algorithm was adopted for the numerical simulations. Gradient reconstruction was performed using the Green–Gauss node-based method. For discretization, a second-order scheme was applied for pressure, whereas the QUICK scheme was used for density and momentum equations.

Turbulence model

In supersonic gas flows, inertial forces substantially exceed viscous forces owing to the high flow velocities, leading to large Reynolds numbers and the development of turbulence. Consequently, numerical analysis of cold spray gas dynamics is commonly based on the Reynolds-averaged Navier–Stokes (RANS) equations, which require an appropriate turbulence closure model. The available turbulence models incorporate empirical coefficients calibrated for particular flow regimes, and their predictive capability is generally restricted to the conditions under which these coefficients were established.

In the present study, the RNG k-ε model was adopted because it offers a favorable balance between computational efficiency and prediction accuracy for cold spray gas-flow simulations.

Particle motion and heating

The velocity of powder particles during the cold gas dynamic spraying process is determined using the following equation [24].

$$m_p \frac{dV_p}{dt} = \frac{1}{2} C_D \rho_g A_p \left(V_g - V_p\right)^2 + F_b, \qquad (10)$$

where $m_p, V_p, C_D, \rho_g, V_g, A_p$, and F_b are particle mass, drag coefficient, particle velocity, particle density, gas velocity, particle cross-sectional area, and body forces, respectively.

Reference [24] provides the necessary relationships for calculating the Reynolds and Mach numbers for a particle.

$$Re_p = \frac{\rho_g |V_g - V_p|}{\mu_g} \qquad (11)$$

and

$$M_p = \frac{|V_g - V_p|}{c} = \frac{|\Delta V|}{\sqrt{\gamma R_g T_g}}. \qquad (12)$$

In this context, the subscript 'g' stands for "gas" and the subscript 'p' stands for "particle." The term "dynamic viscosity" of the gas is represented by μ_g.

$$\mu = \frac{C_1 T_f^{3/2}}{T_f + C_2}, \qquad (13)$$

where C_1 and $C_2 = 1{,}663 \cdot 10^{-5}$ kg/m·s·K$^{1/2}$.

The particle's acceleration can be determined by applying the ideal gas law and the equations for the speed of sound (12) and Mach number (13).

$$a_p = \frac{P_0}{2RT_0}\left(1 + \frac{\gamma - 1}{2} M^2\right)^{-\frac{-1}{\gamma - 1}} \times$$
$$\times \left(M\sqrt{\gamma R T_0 \left(1 + \frac{\gamma-1}{2} M^2\right)^{-1}} - V_p\right)^2 C_D \frac{A_p}{2Vol_p \rho_p}. \qquad (14)$$

Accurate prediction of particle velocity in the cold spray (CS) process depends on the reliable evaluation of the drag coefficient over a wide range of flow regimes.

The temperature of particles transported by the CS gas flow is determined from the average convective heat transfer coefficient, taking into account the flow characteristics in the vicinity of the particle surface. Following the approach presented in [24], the heat exchange at the particle surface can be expressed as:

$$q = \bar{h} A_s \left(T_w - T_p\right) \qquad (15)$$

and

$$\bar{h} = \frac{1}{A_s} \int_{A_s} h dA_s, \qquad (16)$$

where As denotes the particle surface area, and Tw is the gas temperature at the boundary-layer interface (wall).

According to reference [24], the Nusselt number – a non-dimensional temperature gradient – can be evaluated using the following equation:

$$\overline{Nu} = \frac{\bar{h} d_p}{k_g}, \overline{Nu} = f\left(Re_p, M_p, Pr\right), \qquad (17)$$

where k_g is the thermal conductivity of the gas, d_p is the particle diameter.

The convective heat transfer coefficient can be determined from the Nusselt number. To simplify cold spray simulations, the Ranz-Marshall correlation is frequently employed.

$$Nu = 2 + 0.6\, Re^{0.5}\, Pr^{0.33}, \qquad (18)$$

where Pr is the Prandtl number.

The recovery temperature is evaluated within the boundary layer surrounding the particle during its flight.

$$T_r = T_g \left(1 + r\frac{\gamma-1}{2} M_p^2\right), \qquad (19)$$

where r is the recovery factor, whose value for gases is generally close to unity [24].

For Reynolds numbers of approximately 2000, the recovery factor may be evaluated through appropriate empirical relations as follows:

$$r = \frac{\sqrt{\left(\frac{\mu_{g,f} c_{p(g,f)}}{k_{g,f}}\right)}}{\sqrt{Pr}}, \tag{20}$$

where Pr denotes the Prandtl number, and k_g denotes the temperature-dependent thermal conductivity of the gas, which is evaluated using the following relation [25]:

$$k = \frac{9\gamma - 5}{4} \frac{c_V}{\pi d^2} \sqrt{\frac{M k_B T_r}{N\pi}}, \tag{21}$$

where N is Avogadro's constant, $N = 6{,}022 \cdot 10^{23}$ mol^{-1}, k_B denotes Boltzmann constant, $k_B = 1{,}381 \cdot 10^{-2}$ J K^{-1}, d corresponds to the molecular diameter of the gas, and M is the molar mass of the gas species.

2.2. Nozzle design methodology

Conical and MOC nozzle design

The computational procedure for cold gas dynamic spraying (CGDS) begins with selecting the working gas; the gas constant R and the specific heat ratio γ are automatically provided by the program. Subsequently, the material of the particles to be deposited is defined, and its physical and thermophysical properties, such as tensile strength σ, particle density ρ_p, specific heat capacity c_p, melting temperature T_m, as well as the mechanical and thermal calibration factors, are automatically supplied.

The nozzle parameters, including the throat diameter, exit diameter, and nozzle length, are specified, together with the total (stagnation) temperature, T_0, and the corresponding stagnation pressure, P_0. Based on these inputs, the throat gas temperature T^*, velocity v^*, stagnation density ρ_0, throat density ρ^*, throat pressure P^*, and gas mass flow rate $\dot{m}_v$ are calculated as follows. The particle diameter and the impact temperature T_i are then introduced as additional input parameters.

Subsequently, the nozzle cross-sectional areas at the throat and exit are determined, followed by calculating the Mach number at the nozzle exit M_e. The exit gas pressure P_e, temperature T_e, velocity v_e, and density ρ_e are obtained as follows. Using these results, the particle velocity v_p, critical velocity v_{crit}, and the shock pressure P_s are computed.

The results are then verified. If the calculated particle velocity is lower than the critical velocity, the input parameters must be adjusted. For cost-effectiveness, the recommended sequence of modifications is stagnation pressure, stagnation temperature, particle diameter, working gas type, and nozzle geometry. If the particle velocity exceeds the critical value, the procedure advances to further validation. At this stage, the difference between the gas and particle velocities is examined and should be approximately equal to the speed of sound. Additionally, it must be confirmed that no shock waves form inside the nozzle. If the shock pressure is lower than the ambient pressure, the input parameters must be modified again. Conversely, if the shock pressure is greater than the ambient pressure, the calculated particle velocity may be considered valid and sufficient to meet the CGDS deposition requirements.

After verifying and validating the computational results of the CGDS process, the detailed geometric design of the nozzle itself is examined. While the previous section focused on the thermodynamic and fluid dynamic parameters that define the gas-particle interaction within the nozzle, the actual nozzle contour is constructed in the next step. This design determines the gas expansion efficiency and, consequently, the particle acceleration to the desired velocities.

The calculation process begins with specifying the required Mach number at the nozzle exit, followed by setting the length of the divergent part of the nozzle, the specific heat ratio, the number of characteristic lines, and the nozzle throat radius. Next, the Prandtl-Meyer function is determined for the given Mach number using its inverse, and the maximum wall angle of the duct with respect to the flow direction is calculated. This angle is half the Prandtl-Meyer function value for the designed exit Mach number. The flow expansion is represented by a finite number of right-running characteristics, each turning the flow direction by an incremental angle equal to the maximum wall angle divided by the number of characteristics. Then, Prandtl-Meyer constants are computed, followed by calculating angles, Mach numbers, and Mach angles along oblique lines. The coordinates of the contour points are determined using geometric intersection principles. Finally, these points are plotted and connected to generate the nozzle shape.

Computational mesh

The simulations were conducted using the calculated nozzles. A computational polyhedral mesh was employed with refinement applied near the throat, walls, and exit to capture key flow features. A near-wall mesh refinement strategy was implemented to accurately capture the turbulent boundary layer and viscous effects near the solid walls. The height of the first cell adjacent to the wall was fixed at 5 µm, with subsequent layers were expanded at a growth rate of 1.2. The generated mesh's structural integrity was strictly monitored: the minimum orthogonal quality was maintained above 0.7, and the maximum aspect ratio was kept below 30. Based on the results of a comprehensive grid independence study, the final computational grids contained 2105213 and 3084817 elements for the conical and MOC-based nozzles, respectively. This resolution provided an optimal balance, ensuring high accuracy in regions with severe gas-dynamic gradients while incurring low computational cost.

 ISSN 1814-4225 (print)
ISSN 2663-2012 (online)

A strict convergence criterion was applied to the numerical solution. The iterative process was continuously monitored by the reduction in scaled residuals, with target values set below 10^{-6} for the energy equation and strictly below 10^{-5} for the continuity, momentum, and turbulence parameters [26]. Additionally, global mass conservation was tracked along with the stabilization of physical properties (e.g., temperature and velocity) at the nozzle exit. The computational process was considered fully converged and terminated only when the monitored physical variables reached a steady state with 1% fluctuations [26].

Computational domain and boundary conditions

Numerical simulations of the gas–particle flow through a supersonic nozzle and in the downstream free jet were carried out using ANSYS Fluent 2025 R1. The problem is described as a 2D axisymmetric model that accounts for turbulent gas flow and the presence of a dispersed phase represented by solid powder particles. Figure 1 illustrates the computational domain and the corresponding boundary conditions.

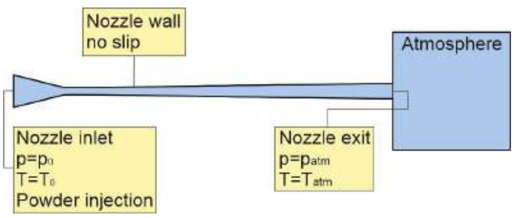

Fig. 1: The computational domain and boundary conditions

3. Results and Discussion

Cold spray nozzle design

The nozzles were designed for operation using air as the operating gas and maintain the gas flow rate under 60 m^3/h. For this reason, optimization tasks were performed to select an appropriate nozzle geometry for the following gas initial conditions: stagnation pressure of 2.5 MPa, stagnation temperature of 650 °C, and aluminum powder with a mean particle diameter of 25 μm. The nozzles were successfully designed (Fig. 2) and validated using the CFD methodology.

Matlab code was used to design the MOC cold spraying nozzle geometry using the adopted Method of Characteristics.

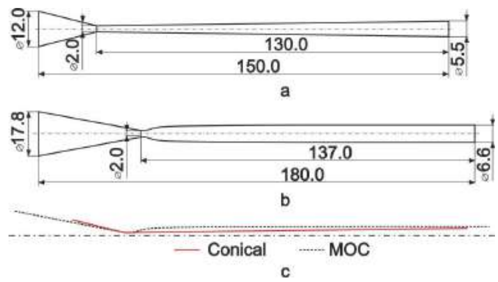

Fig. 2. Calculated cold spray nozzles geometry:
a – Conical nozzle; b – MOC nozzle; c – nozzle profiles

This code generates the geometry of a bell-shaped convergent-divergent nozzle and optimizes the operation modes. The nozzle design is based on a desired Mach number that is most appropriate for particle acceleration, accounting for the boundary layer on the nozzle walls.

Gas flow results

Simulations were conducted for a 2-Dimensional plane of the nozzle for stagnation temperatures 650 ˚C and pressures 2.5 MPa.

Figure 3 illustrates the predicted gas velocity distribution in the meridional plane for the conical and MOC nozzles.

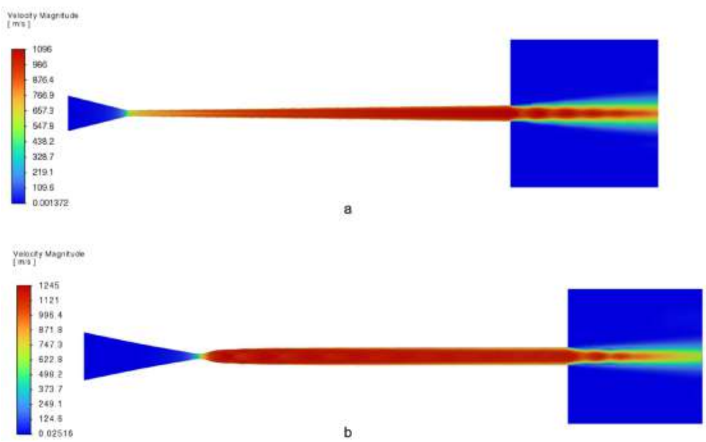

Fig. 3. Color of the velocity for the carrier phase: a – Conical nozzle; b – MOC nozzle

Both nozzles operate in an underexpanded regime, indicating that the gas exits the nozzles at pressures higher than the ambient pressure. Upon exit, the flow undergoes a Prandtl-Meyer expansion to adapt to the surrounding conditions. This expansion is followed by a compression wave in the shear layer of the jet, where the pressure matches the ambient level. The MOC nozzle exhibits a more uniform velocity distribution and a higher exit velocity, which contributes to more efficient particle acceleration at the same gas flow rate.

The expansion waves are more pronounced in a conical nozzle, indicating that the jet decelerates more under identical operating conditions.

The exit gas velocity for the MOC nozzle reaches 1408.51 m/s, which is 14.81 m/s higher than that of the conical nozzle.

A comparative analysis of the vorticity magnitude contours was also conducted for both nozzle types. The results show that vorticity is generated in the boundary layer along the nozzle walls and is more intense in the MOC nozzle. In supersonic flows, boundary layers typically exhibit significant vorticity due to viscous effects near solid walls. However, the thick turbulent boundary layer in the MOC nozzle does not appear to significantly influence the magnitude of vorticity within the shear layer of the jet. In addition, a localized region of increased vorticity is observed in the shock interaction zone of the MOC nozzle.

Fig. 4 shows the flow properties (static pressure, static temperature, and velocity magnitude) along the nozzle throat for both the conical and MOC configurations.

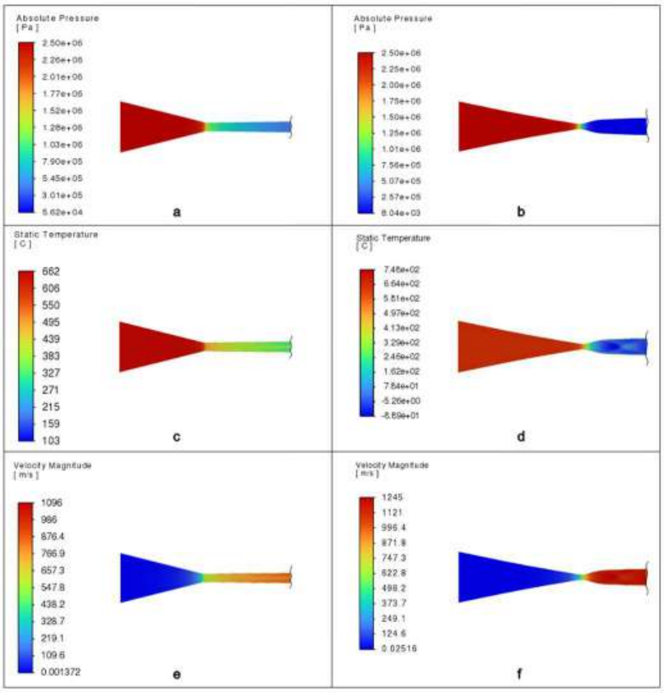

Fig. 4. Gas flow characteristics for the Conical (left side) and MOC (right side) nozzles at the throat:
a and b – absolute pressure; c and d – static temperature; e and f – velocity

As hot gas flows through the conical nozzle, both static pressure and temperature gradually and nearly linearly decrease along the jet axis. Analysis of the flow characteristics along the centerline reveals oscillations near the nozzle exit, which are attributed to alternating shock waves and expansion fans.

In contrast, the MOC-type nozzle exhibits a sharp drop in the static pressure and temperature immediately after the flow passes through the throat. This indicates a more intense and rapid gas expansion compared with the conical geometry.

As shown in Fig. 4, the velocity of the carrier gas phase in the MOC nozzle significantly changes. The acceleration of the gas and consequently, the increase in Mach number occurs earlier in the flow, enabling aluminum particles to experience high drift velocities sooner as the gas expands. This is crucial for system performance because it reduces the velocity lag between the particles and the gas. As a result, the particles can reach or exceed their critical velocity before exiting the nozzle, facilitating their effective deposition onto the target substrate.

Discrete phase results

This study analyzed the acceleration dynamics of 25 μm aluminum particles within the MOC and conical nozzles. Figure 5 presents the trajectories of powder particles, colored according to their velocity, within the supersonic nozzle and the downstream free-jet region for a gas stagnation pressure of 2.5 MPa and a stagnation temperature of 650 °C.

Under identical inlet gas conditions, aluminum particles attain higher velocities in the MOC nozzle than in the conical nozzle. The particle velocity distribution at the exits of both nozzles is shown in Fig. 6.

Figure 6 demonstrates that the MOC nozzle achieves a more uniform particle acceleration within the velocity range of 590 to 732 m/s. Since the peak particle velocity directly correlates with their kinetic energy, this suggests a greater potential for intense plastic deformation upon impact, which can enhance the metal deposition quality.

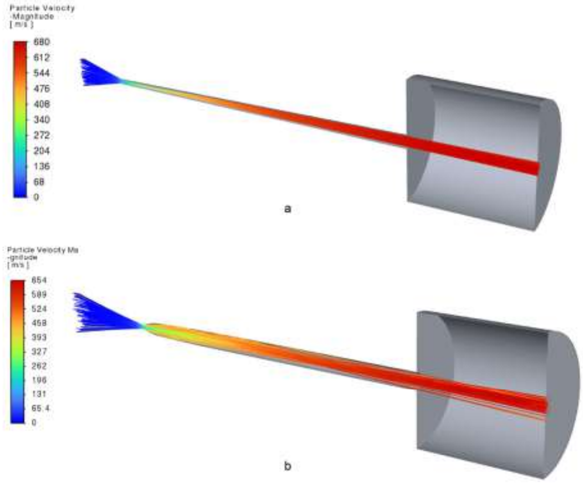

Fig. 5. Particles track colored according to their velocity magnitude: a – Conical nozzle; b – MOC nozzle

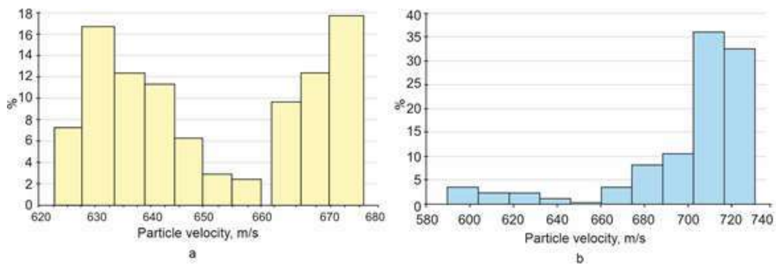

Fig. 6. Particle velocity distribution at nozzle exit:
a – Conical nozzle; b – MOC nozzle

Table 1 summarizes the simulation results for the investigated nozzle geometries and compares their key gas-dynamic and kinematic characteristics.

Table 1
A comparison of key performance characteristics between conical and MOC-based nozzles

Parameter	Conical Nozzle	MOC Nozzle
Maximum exit gas velocity at nozzle exit, m/s	1393.7	1408.51
Average particle velocity at nozzle exit, m/s	676	732
Flow uniformity (particle acceleration)	Lower (wider velocity spread)	Higher (narrower velocity spread)
Free jet structure stability	Lower (pronounced expansion waves)	Higher (more stable shear layer)
Vorticity generation in the boundary layer	Moderate	Intense

As summarized in Table 1, the MOC-based nozzle demonstrates superior momentum transfer efficiency. The rapid gas expansion in the MOC-based design ensures earlier and more uniform acceleration of approximately 70% of the discrete phase, with a velocity distribution of 700…730 m/s (for a conical nozzle: 40% within 660…675 m/s), ultimately leading to a narrower particle-velocity distribution and a more stable free-jet structure. These factors are critical for minimizing the velocity lag between phases and maximizing the deposition efficiency during cold spraying.

CFD model validation

The numerical model, meshing strategy, and physical sub-models (including the RNG k-ε turbulence model and discrete-phase interactions) employed in this study were validated by replicating the computational conditions and comparing CFD results with experimental data for a supersonic cold spray nozzle, as originally reported by Nastic and Jodoin [26]. Particle streak velocimetry (PSV), particle tracking velocimetry (PTV), and the Cold Spray Meter (CSM) were used to measure particle velocities in the gas flow.

Table 2 shows that the relative deviation of our replicated simulation results from the baseline numerical model ranges from 6.3% to 7.8%. Furthermore, the calculated CFD values fall within or near the interquartile range of the experimentally recorded velocities (particularly for the PSV method, where the deviation from the mean is only 7.3–11.4%). These deviations between the CFD results and experimental data are attributed to the stochastic nature of particle motion in supersonic flows and measurement uncertainties. Because the current study employs this validated CFD methodology under similar gas-dynamic regimes (comparable Mach and Reynolds numbers), the chosen modeling approach is considered highly reliable and fully adequate for predicting the carrier gas flow characteristics and particle acceleration dynamics in the investigated conical and MOC nozzle configurations.

Table 2

Comparison of the calculated particle velocities with experimental data and baseline numerical results [26]

Velocity diagnostic method	Gas stagnation pressure, K	Interquartile range (mean experimental velocity), m/s	Baseline CFD velocity, m/s	Current study CFD velocity, m/s	Deviation from baseline CFD, %	Deviation from mean exp., %
CSM	473	155–215 (184)	140	131.2	6.3	28.7
	773	160–230 (193)	171	157.6	7.8	18.3
PSV	473	125–175 (148)	140	131.2	6.3	11.4
	773	150–195 (170)	171	157.6	7.8	7.3
PTV	473	155–180 (169)	140	131.2	6.3	22.4
	773	170–190 (177)	171	157.6	7.8	11.0

Discussion

The comparative analysis demonstrated several advantages of using MOC-based nozzle over a conical convergent-divergent one for CGDS. The primary advantage is improved momentum-transfer efficiency from the gas to the powder particles. The MOC-based nozzle geometry promotes earlier adiabatic expansion of the working gas, enabling 25 µm-diameter aluminum particles to reach an average velocity of 732 m/s, compared to 676 m/s in the conical nozzle under identical gas stagnation conditions (pressure of 2.5 MPa and temperature of 650 °C). Furthermore, the MOC-based nozzle provides a significantly narrower velocity spread: almost 70% of the particles are concentrated in the 700–730 m/s range. This allows for maintaining a more uniform kinetic energy distribution upon particle impact with the substrate, which is a critical prerequisite for the stability and repeatability of the coating deposition process.

Despite the promising results obtained, the current study has certain limitations that should be acknowledged. First, the numerical analysis was conducted using a two-dimensional axisymmetric model based on the RANS equations. Although this approach is computationally efficient and widely used to predict mean flow characteristics and powder particle velocities in the CGDS process, it inherently limits the investigation of complex three-dimensional turbulent structures and asymmetric flow instabilities. Second, the discrete phase modeling assumed perfectly spherical 25 µm particles of uniform size, without accounting for the morphological characteristics and size distribution of the feedstock powder. The obtained results require further empirical verification. The next stage of research will involve manufacturing the conical and MOC nozzles to conduct experimental testing, evaluate flow and particle velocities, and perform coating deposition and its subsequent analysis.

4. Conclusions

This study provides a deeper understanding of key design parameters and their impact on nozzle design for cold gas dynamic spraying. For the first time, a two-dimensional axisymmetric CFD model was applied to numerically analyze the two-phase gas-particle flow in the developed conical and MOC nozzles. The results demonstrated that under the same inlet gas conditions, the MOC nozzle ensures more uniform particle acceleration and higher impact particle velocities than the conical nozzle. This indicates the potential of the MOC design to enhance the cold spray process efficiency.

Further application of the MOC-based design methodology allows for the adaptation and optimization of nozzle geometry to meet the specific requirements of various applications, making this approach versatile and flexible. Moreover, CFD modeling is a powerful tool for numerical testing and improving nozzle designs, significantly reducing the need to manufacture expensive physical prototypes and conduct numerous experiments. The model helps identify optimal operating conditions that reduce costs and improve coating quality by enabling the prediction of gas-flow parameters and particle behavior.

However, the numerical results presented in this work require further validation through experimental studies to confirm the CFD model's enhanced performance of cold spray nozzles. Additionally, verifying the accuracy of the modeled gas flow characteristics and particle dynamics is important to ensure full alignment between theoretical predictions and real processes. Overall, this study lays a solid foundation for further optimization of cold spray technology and the implementation of innovative solutions in the field. Furthermore, based on the established comparative methodology, this geometric analysis will be expanded into a comprehensive parametric study that investigates the combined effects of operating pressures, stagnation temperatures, and particle size distributions on the performance of MOC-based nozzles.

Contributions of authors: supervision – **Olga Shypul,** conceptualization – **Oleksandr Shorinov;** methodology – **Nina Savchenko, Oleksandr Shorinov;** data curation – **Oleh Tryfonov, Nina Savchenko;** validation – **Oleksandr Shorinov, Olga Shypul;** original draft preparation – **Nina Savchenko;** review and editing – **Oleksandr Shorinov.**

All authors have read and approved the final manuscript for publication.

Conflict of Interest

The authors declare that they have no conflict of interest in relation to this research, whether financial, personal, authorship or otherwise, that could affect the research and its results presented in this paper.

Financing

This study was conducted without financial support.

Data Availability

The manuscript has no associated data.

Use of Artificial Intelligence

The authors confirm that they did not use artificial intelligence or AI-assisted technologies in the preparation, writing, or editing of this manuscript.

References

1. Dykhuizen, R. C., & Smith, M. F. Gas dynamic principles of cold spray. *Journal of Thermal Spray Technology*, 1998, vol. 7, no. 2, pp. 205–212. DOI: 10.1361/105996398770350945.

2. Bernard, C. A., Takana, H., Lame, O., Ogawa, K., & Cavaillé, J.-Y. Influence of the nozzle inner geometry on the particle history during cold spray process. *Journal of Thermal Spray Technology*, 2022, vol. 31, no. 7, pp. 1–15. DOI: 10.1007/s11666-022-01407-y.

3. Grujicic, M. J., DeRosset, W. S., & Helfritch, D. Flow analysis and nozzle-shape optimization for the cold-gas dynamic-spray process. *Proceedings of the Institution of Mechanical Engineers, Part B: Journal of Engineering Manufacture*, 2003, vol. 217, no. 11, pp. 1603–1613. DOI: 10.1243/095440503771909980.

4. Shorinov, O., Volkov, A., Dolmatov, A., & Balushok, K. Numerical Simulation of a Modified Nozzle for Cold Spraying. *Advanced Manufacturing Processes V. InterPartner 2023, Lecture Notes in Mechanical Engineering*, Springer, Cham, 2024, pp. 563–575. DOI: 10.1007/978-3-031-42778-7_53.

5. Shorinov, O. V., & Polyviany, S. A. Simulation of Gas Flow with Nanocomposite Carbon-Containing Powders in Supersonic Nozzle. *Metallofizika i Noveishie Tekhnologii*, 2022, vol. 44, no. 5, pp. 601–611. DOI: 10.15407/mfint.44.05.0601.

6. Gabor, T., Akin, S., & Jun, M. B.-G. Numerical studies on cold spray gas dynamics and powder flow in circular and rectangular nozzles. *Journal of Manufacturing Processes*, 2024, vol. 114, pp. 232–246. DOI: 10.1016/j.jmapro.2024.02.005.

7. Sakaki, K. The influence of nozzle design in the cold spray process. *The Cold Spray Materials Deposition Process: Fundamentals and Applications*, Woodhead Publishing, 2007, pp. 117–126. DOI: 10.1533/9781845693787.2.117.

8. Grujicic, M. J., Zhao, C. L., Tong, C., Derosset, W. S., & Helfritch, D. Analysis of the impact velocity of powder particles in the cold-gas dynamic-spray process. *Materials Science and Engineering: A*, 2004, vol. 368, no. 1–2, pp. 222–230.

9. Karimi, M., Fartaj, A., Rankin, G., Vanderzwet, D., Birtch, W., & Villafuerte, J. Numerical simulation of the cold gas dynamic spray process. *Journal of Thermal Spray Technology*, 2006, vol. 15, no. 4, pp. 518–523.

10. Raoelison, R. N., Koithara, L. L., Costil, S., & Langlade, C. Turbulences of the supersonic gas flow during cold spraying and their negative effects: A DNS CFD analysis coupled with experimental observation and laser impulse high-speed shadowgraphs of the particles in-flight flow. *International Journal of Heat and Mass Transfer*, 2020, vol. 147, article no. 118894. DOI: 10.1016/j.ijheatmasstransfer.2019.118894.

11. Krampe, M., & Kuhlenkötter, B. Experimental investigation of the influence of different nozzle exit geometries on the depositing of strands in fused layer modeling. *Annals of Scientific Society for Assembly, Handling and Industrial Robotics 2023*, 2023, pp. 13–25. DOI: 10.1007/978-3-031-74010-7_2.

12. Alonso, L., Garrido-Maneiro, M. A., & Poza, P. A study of the parameters affecting the particle velocity in cold-spray: Theoretical results and comparison with experimental data. *Additive Manufacturing*, 2023, vol. 67, article no. 103479. DOI: 10.1016/j.addma.2023.103479.

13. Kun, T., Wenjie, H., & Yurong, W. Optimization of cold spray nozzles based on the response surface methodology. *Journal of Engineering Sciences*, 2024, vol. 11, no. 1, pp. F1–F11. DOI: 10.21272/jes.2024.11(1).f1.

14. Gutiérrez de Frutos, J., List, A., Nielsen, S., Gärtner, F., & Klassen, T. Nozzle geometry evaluation for cold spray applications by using 3D-CFD

calculations. *Journal of Thermal Spray Technology*, 2025, vol. 34, no. 3, pp. 570–586. DOI: 10.1007/s11666-025-01945-1.

15. Sakaki, K., Huruhashi, N., Tamaki, K., & Shimizu, Y. Effect of nozzle geometry on cold spray process. *Proceedings of the International Thermal Spray Conference (ITSC 2002)*, ASM International, March 2002, pp. 385–392. DOI: 10.31399/asm.cp.itsc2002p0385.

16. Sharma, A. K., Vashishtha, A., Callaghan, D., Bakshi, S. R., Kamaraj, M., & Raghavendra, R. CFD investigation of a co-flow nozzle for cold spray additive manufacturing applications. *Journal of Thermal Spray Technology*, 2024, vol. 33, no. 7, pp. 1251–1269. DOI: 10.1007/s11666-024-01764-w.

17. Grass Nunez, J. S., Rojas Perilla, D. A., Barragan De Los Rios, G. A., & Coelho, R. T. Numerical and experimental analysis of gas flow in a coaxial nozzle applied to directed energy deposition (DED). *International Journal of Engineering Materials and Manufacture*, 2021, vol. 6, no. 3, pp. 102–113. DOI: 10.26776/ijemm.06.03.2021.01.

18. Hu, W. J., & Shorinov, O. Optimization of technological parameters for cold spraying using the response surface method. *Journal of Engineering Sciences*, 2024, vol. 11, no. 2, pp. F1–F8. DOI: 10.21272/jes.2024.11(2).f1.

19. Murphy, J., Schmidt, D., Wang, S. P., & Corradini, M. L. Multi-dimensional modelling of multiphase flow physics: high speed nozzle and jet flows — a case study. *Nuclear Engineering and Design*, 2001, vol. 204, no. 1–3, pp. 177–190. DOI: 10.1016/S0029-5493(00)00362-9.

20. Alonso, L., Garrido, M. Á., & Poza, P. An optimisation method for the cold-spray process: On the nozzle geometry. *Materials & Design*, 2022, vol. 214, article no. 110387. DOI: 10.1016/j.matdes.2022.110387.

21. Yin, S., Sun, Y., Wang, X., Guo, Z., & Liao, H. Effect of spray angle on temperature distribution within the metallic substrate in cold spraying. *Journal of Thermal Spray Technology*, 2013, vol. 22, no. 6, pp. 983–991. DOI: 10.1007/s11666-013-9931-x.

22. Nastic, A., Jodoin, B., Poirier, D., & Legoux, J. G. Particle temperature effect in cold spray: A study of soft particle deposition on hard substrate. *Surface and Coatings Technology*, 2021, vol. 406, article no. 126735. DOI: 10.1016/j.surfcoat.2020.126735.

23. Tabbara, H., Gu, S., McCartney, D. G., Price, T. S., & Shipway, P. H. Study on Process Optimization of Cold Gas Spraying. *Journal of Thermal Spray Technology*, 2010, vol. 20, no. 3, pp. 608–620. DOI: 10.1007/s11666-010-9564-2.

24. Nastic, A., MacDonald, D., & Jodoin, B. The influence of feedstock powder. *Materials Forming, Machining and Tribology*, Cham: Springer International Publishing, 2020, pp. 33–85. DOI: 10.1007/978-3-030-42756-6_3.

25. Yin, S., Cavaliere, P., Aldwell, B., Jenkins, R., Liao, H., Li, W., & Lupoi, R. Cold spray additive manufacturing and repair: Fundamentals and applications. *Additive Manufacturing*, 2018, vol. 21, pp. 628–650. DOI: 10.1016/j.addma.2018.04.017.

26. Nastic, A., & Jodoin, B. Evaluation of heat transfer transport coefficient for cold spray through computational fluid dynamics and particle in-flight temperature measurement using a high-speed IR camera. *Journal of Thermal Spray Technology*, 2018, vol. 27, no. 8, pp. 1491–1517. DOI: 10.1007/s11666-018-0787-y.

Received 03.10.2025, Received in revised form 09.04.2026
Accepted date 27.06.2026, Published date 31.07.2026

ЧИСЕЛЬНИЙ АНАЛІЗ ВПЛИВУ ГЕОМЕТРІЇ СОПЛА ДЛЯ ХОЛОДНОГО ГАЗОДИНАМІЧНОГО НАПИЛЮВАННЯ НА ПРИСКОРЕННЯ ЧАСТИНОК

О. В. Шорінов, Н. В. Савченко, О. В. Трифонов, О. В. Шипуль

Предметом *статті є комп'ютерний аналіз впливу геометрії сопла на газодинаміку та прискорення частинок у процесі холодного газодинамічного напилення (ХГН).* ***Метою*** *є порівняння ефективності традиційних конічних сопел та сопел, спроєктованих методом характеристик (МОС), з точки зору їх здатності прискорювати частинки до критичних швидкостей, необхідних для формування якісних покриттів.* ***Завдання****, які необхідно вирішити: спроєктувати та змоделювати конічні та МОС-сопла; провести моделювання стисливих двофазних газо-частинкових потоків у цих геометріях; проаналізувати розподіли швидкості, тиску та температури вздовж сопла та в зоні струменя; оцінити ефективність прискорення та розподіл швидкостей алюмінієвих частинок.* ***Методи дослідження:*** *чисельне моделювання газо-частинкового потоку на основі рівнянь Нав'є–Стокса з використанням турбулентної моделі RNG* $k-\varepsilon$ *в ANSYS Fluent 2025 R1, у поєднанні з лагранжевим відстеженням частинок; комп'ютерне проєктування сопел у MATLAB із застосуванням методу характеристик; порівняння полів течії та динаміки частинок для різних конфігурацій сопел.* ***Отримані результати*** *показують, що обидва сопла працюють у режимі недорозширеного струменя, проте сопло МОС-сопло забезпечує більш раннє прискорення робочого газу та частинок, що призводить до більш рівномірного поля швидкостей та зменшення відставання швидкості частинок від газу. Для алюмінієвих частинок діаметром 25 мкм МОС-сопло забезпечує досягнення вищих значень швидкості порівняно з конічним соплом, що свідчить про підвищений потенціал пластичної деформації та покращення міцності зчеплення покриття з підкладкою. Крім того, у МОС-соплі зафіксовано вищі швидкості на виході та стабільнішу структуру струменя.* ***Висновки.*** *Наукова новизна отриманих* *результатів полягає у встановленні закономірності прискорення газового потоку з частинками алюмінієвого порошку в конічному і МОС-соплах, оптимізованих для напилювання алюмінію при тиску газу 2,5 МПа і температурі 650 °С. Доведено, що МОС-сопло забезпечує більш раннє розширення газу та стабільнішу структуру вільного струменя, що дозволяє досягти вищої й значно рівномірної швидкості частинок порошку порівняно з конічним соплом за однакових умов напилювання.*

Ключові слова*: CFD-моделювання, математичне моделювання, газовий потік, надзвукове сопло, ANSYS Fluent, напилювання, покриття.*

Шорінов Олександр Володимирович – канд. техн. наук, доц., доц. каф. технології виробництва авіаційних двигунів, Національний аерокосмічний університет «Харківський авіаційний інститут», Харків, Україна.

Савченко Ніна Валеріївна – канд. фіз.-мат. наук, доц., зав. каф. вищої математики та системного аналізу, Національний аерокосмічний університет «Харківський авіаційний інститут», Харків, Україна.

Трифонов Олег Валерійович – канд. техн. наук, доц., доц. каф. технології виробництва літальних апаратів, Національний аерокосмічний університет «Харківський авіаційний інститут», Харків, Україна.

Шипуль Ольга Володимирівна – доктор техн. наук, проф., проф. кафедри технології виробництва літальних, Національний аерокосмічний університет «Харківський авіаційний інститут», Харків, Україна.

Oleksandr Shorinov – Candidate of Technical Sciences, Associate Professor, Associate Professor at the Department of Aircraft Engines Manufacturing Technology, National Aerospace University "Kharkiv Aviation Institute", Kharkiv, Ukraine,
e-mail: o.shorinov@khai.edu, ORCID: 0000-0002-5057-6679, Scopus Author ID: 57223082183.

Nina Savchenko – Candidate of Physical and Mathematical Sciences, Associate Professor, Head of the Department of Higher Mathematics and System Analysis, National Aerospace University "Kharkiv Aviation Institute", Kharkiv, Ukraine,
e-mail: n.savchenko@khai.edu, ORCID: 0000-0001-8144-9368, Scopus Author ID: 56421771100.

Oleg Tryfonov – Candidate of Technical Sciences, Associate Professor, Associate Professor at the Department of Aircraft Production Technology, National Aerospace University "Kharkiv Aviation Institute", Kharkiv, Ukraine,
e-mail: o.tryfonov@khai.edu, ORCID: 0000-0001-8058-8649, Scopus Author ID: 57192959255.

Olga Shypul – Doctor of Technical Sciences, Professor, Professor at the Department of Aircraft Production Technology, National Aerospace University "Kharkiv Aviation Institute", Kharkiv, Ukraine,
e-mail: o.shypul@khai.edu, ORCID: 0000-0002-1356-5831, Scopus Author ID: 57192959380.